Multi-objective Robust Optimal Secure Operation Model of Large-scale Power Grid with Multiple Back-to-back Voltage Source Converter Based Systems Considering Short-circuit Current Limitation

Weikun Liang, Shunjiang Lin, Yuerong Yang, Ziqing Yang, and Mingbo Liu

***Abstract*—With the load growth and the power grid expansion, the problem of short-circuit current (SCC) exceeding the secure limit in large-scale power grids has become more serious, which poses great challenge to the optimal secure operation. Aiming at the SCC limitations, we use multiple back-to-back voltage source converter based (B2B VSC) systems to separate a large-scale AC power grid into two asynchronous power grids. A multi-objective robust optimal secure operation model of large-scale power grid with multiple B2B VSC systems considering the SCC limitation is established based on the AC power flow equations. The decision variables include the on/off states of synchronous generators, power output, terminal voltage, transmission switching, bus sectionalization, and modulation ratios of B2B VSC systems. The influence of inner current sources of renewable energy generators on the system SCC is also considered. To improve the computational efficiency, a mixed-integer convex programming (MICP) framework based on convex relaxation methods including the inscribed *N*-sided approximation for the nonlinear SCC limitation constraints is proposed. Moreover, combined with the column-and-constraint generation (C&CG) algorithm, a method to directly solve the compromise optimal solution (COS) of the multi-objective robust optimal secure operation model is proposed. Finally, the effectiveness and computational efficiency of the proposed solution method is demonstrated by an actual 4407-bus provincial power grid and the modified IEEE 39-bus power grid, which can reduce the consumed CPU time of solving the COS by more than 90% and obtain a better COS.**

***Index Terms*—Large-scale power grid, optimal secure operation, short-circuit current(SCC) limitation, back-to-back, voltage source converter, convex relaxation, multi-objective robust optimization.**

Manuscript received: March 25, 2024; revised: June 23, 2024; accepted: August 29, 2024. Date of CrossCheck: August 29, 2024. Date of online publication: October 24, 2024.

This work was supported by the National Natural Science Foundation of China (No. 51977080).

W. Liang, S. Lin (corresponding author), Y. Yang, Z. Yang, and M. Liu are with the School of Electric Power Engineering, South China University of Technology, Guangzhou 510640, China (e-mail: 3012273545@qq. com; linshj@scut. edu. cn; 1078533567@qq.com; 1781419055@qq.com; epmbliu@scut.edu.cn).

DOI: 10.35833/MPCE.2024.000328

NOMENCLATURE

A. Sets and Indices

Ω_G, Ω_{RE}, Ω_L	Sets of buses with synchronous generators, renewable energy stations (RESs), and loads
Ω_{ij}	Set of branches in independent circuit
Ω_k	Set of branches for transmission switching or bus sectionalization
Ω	Box uncertainty set of RES output
i, j, f	Indices of AC buses in power grid
k	Index of branches
n	Number of AC buses in power grid
n_c	Number of three-phase short-circuit faults of critical buses required to be considered
X	Feasible region of multi-objective robust optimization model
0	Initial value
max, min	Upper and lower bounds

B. Variables

$\varsigma_l=[\varsigma_{lk}]$	Vector of binary variables, $\varsigma_{lk}=1$ if switching line k is open; otherwise, $\varsigma_{lk}=0$
$\varsigma_g=[\varsigma_{gi}]$	Vector of binary variables, $\varsigma_{gi}=1$ if generator at bus i is shut-down; otherwise, $\varsigma_{gi}=0$
φ_{ci}	Power factor angle of voltage source converter (VSC) station connected to bus i
θ_{ij}	Voltage phase difference between buses i and j
δ_i	Phase difference between V_i and V_{ci}
ς_X, ς_R	Binary variables equal to 1 if X_{ff} and R_{ff} are positive, respectively
ξ_{ijb}	Binary variable, $\xi_{ijb}=1$ if modulation ratio is at the b^{th} discrete gear value; otherwise, $\xi_{ijb}=0$
$\Delta\boldsymbol{Y}_v=[\Delta Y_{v,ij}]$	Change matrix of admittance considering back-to-back voltage source converter based (B2B VSC) systems
d_+, d_-	Normalized distances from the optimal solution to utopia and nadir points

d_0	Normalized distance between utopia and nadir points
M_i	Modulation ratio of VSC station connected to bus i
P_{Gi}, Q_{Gi}	Active and reactive power of generator at bus i
P_{REi}, Q_{REi}	Active and reactive power of RES at bus i
P_{Li}, Q_{Li}	Active and reactive load power of bus i
P_{vdi}, Q_{vdi}	Active and reactive power absorbed by VSC station connected to bus i from AC system
S_{vdi}	Apparent power absorbed by VSC station connected to bus i from AC system
U_{vi}, I_{vi}	DC voltage and current of VSC station connected to bus i
V_{ci}	Input AC voltage of VSC station connected to bus i
V_{f0}	Voltage of bus f before occurrence of short-circuit fault
V_i, I_i	Voltage and injected current of bus i
$\boldsymbol{x}$, $\boldsymbol{v}$	Decision variable vector and uncertain variable vector
X_{ff}, R_{ff}	Imaginary and real parts of self-impedance of bus f
X_{fi}, R_{fi}	Imaginary and real parts of mutual impedance between buses f and i
Z_{ff}, Z_{fi}	Self-impedance of bus f and mutual impedance between buses f and i

C. Parameters

α	Margin of checking-adding-checking again-adding again method
α_d, α_u	Downward and upward fluctuation proportions of box uncertainty set
μ_i	DC voltage utilization ratio, generally equal to 0.866
a_{i0}, a_{i1}, a_{i2}	Coefficients of quadratic cost function of generator at bus i
c_k, c_{gi}	Cost coefficients of switching line k and shutdown generator at bus i
c_{wi}	Cost coefficient of curtailment of RES at bus i
$\boldsymbol{E}_f$	Unit vector
G_{ij}, B_{ij}	Mutual conductance and susceptance between buses i and j
$I_{f\max}$	Upper limit of short-circuit capacity for circuit breaker
I_{RE}	Preset value of equivalent constant current source of RES
M	A big positive number
M_{ijb0}	The b^{th} discrete gear value of M_{ij}
$P_{REi,pre}$	Predicted power of RES at bus i
V_{iN}	Rated voltage of bus i
$V_{f\min}$, $V_{f\max}$	Lower and upper bounds of V_{f0}
x_{gi}	Subtransient reactance of generator at bus i
$\boldsymbol{Y}$	Admittance matrix after short-circuit fault
y_i	Admittance of VSC station connected to bus i
y_{ij}	Equivalent admittance between buses i and j

I. Introduction

In recent years, with the rapid growth of electric power load demands, the installed generation capacity continuously increases and the network connection becomes closer, the short-circuit current (SCC) levels in the dense-load areas of large-scale power grids is continuously increasing, and the problem of SCC exceeding the secure limit is becoming more serious [1], [2]. According to statistics [3], Guangdong power grid is the largest and most complex provincial power grid in China and it has the largest receiving loads as a receiving-end power grid, with a maximum power load of 138 million kW in 2022. In addition, the power load demand of the entire Guangdong province is highly concentrated in the Pearl River Delta region, and the SCC level in the dense-load areas has gradually approached or even exceeded the allowable breaking capacity of circuit breakers, seriously threatening the secure operation of power system. To limit the SCC level, three back-to-back voltage source converter based (B2B VSC) systems have been installed to separate this large-scale AC power grid into two asynchronous power grids [4]. Therefore, it becomes imperative to ascertain the most effective methodology to analyze the effect of the three B2B VSC systems on limiting the SCC level and regulate their operation, with the objective of determining the system operation mode that meets the required SCC limitation.

Several studies have focused on the SCC limitation problem in the optimal operation of power grids [5]-[8]. In [5], an optimal transmission switching (TS) linearization model with SCC limitation and $N-1$ reliability is proposed. In [6], a co-optimization model of unit commitment (UC) and TS with SCC limitation is proposed. In [7], a day-ahead scheduling model considering UC and TS is proposed to avoid the excessive SCC problem caused by wind farm integration. In [8], an SCC-constrained optimal model for topology adjustment in long-term operation is proposed, including TS, bus sectionalization (BS), lines operating out of breaker bay, and UC. In addition, the SCC limitation problem has also been studied in the optimal operation of transmission expansion planning [9]-[11]. In [9] and [10], a linear DC power flow model is proposed for transmission network expansion planning with embedded SCC constraints. In [11], an SCC-constrained planning model is proposed to determine the optimal locations and sizes of fault current limiters while considering the TS. However, [5]-[11] all use the DC power flow model to describe the power system operational characteristics, ignoring the influences of generator output, bus voltage amplitude, and line resistance on the SCC level. In [12] and [13], an SCC-constrained expansion planning model obtained by successive linearization technique is proposed, in which the linearized AC power flow model is used to consider the influence of bus voltage amplitude and line resistance on the SCC level. However, the optimal solution of the linearized AC power flow model still has errors compared with that of the accurate nonlinear AC power flow model, resulting in the problem of SCC exceeding the secure limit during the actual power grid operation. For the optimal operation of large-scale power grid considering accurate nonlinear AC power flow model, there is much greater complexity for solving the large-scale mixed-integer nonlinear programming (MINLP) model due to the large number of integer variables and nonlinear constraints involved. It imposes significant challenges to solving this model reliably and efficiently.

To limit the SCC level, the optimal operation modes include BS [8], [10], TS [5]-[9], [11], UC [6]-[8], and bundled conductors of lines [12]. In recent years, some new modes have attracted extensive attention to limit the SCC level. To limit the SCC level of the large-scale power grid, B2B VSC systems have gradually been constructed in the dense-load areas, dividing the large-scale power grid into two small-scale asynchronous power grids. Moreover, compared with AC transmission lines, B2B VSC systems have higher operational flexibility, which can easily adjust the transmission power and bus voltage. However, there has been no literature on using B2B VSC systems to limit the SCC level in the optimal operation of power system till now. It needs further research on coordinately regulating the B2B VSC systems and other modes to limit the SCC level in the optimal operation.

In addition, in the optimal operation models of the above publications [5]-[13], only the single-objective function is considered and the uncertainty of renewable energy station (RES) output is not considered. However, in the actual power grid operation, multiple indicators such as total operation cost, bus voltage deviation, and power loss of the power grid are required to be considered. If only one single objective such as total operation cost is considered, it will result in large voltage deviations and power loss of the obtained optimal operation results. Thus, it is necessary to consider the optimal operation problem with multiple objectives simultaneously. However, the uncertainty of RES output increases the complexity of solving the multi-objective optimal operation model. The commonly-used methods to address the multi-objective optimization problems and RES output uncertainty simultaneously are multi-objective stochastic optimization [14], [15], multi-objective robust optimization [16]-[18], and multi-objective distributionally robust optimization [19], [20], which are applied in the resilience improvement planning of distribution networks [14], active management strategy of distribution networks [15], optimal operation of integrated energy microgrids [16], voltage/var control of distribution networks [17], charging and discharging scheduling of electric vehicles [18], voltage risk management for unbalanced distribution systems [19], and hydrogen-involved renewable energy system planning [20]. The above studies use the weighted sum or ε-constraint methods to address the multi-objective optimization problems, which requires first obtaining massive discrete Pareto optimal solutions (POSs), and then selecting a compromise optimal solution (COS) from the POSs as the optimal decision-making scheme. When weighted-sum or ε-constraint methods are applied to solve the multi-objective stochastic or robust optimization problem of large-scale power grid, the required computational burden and time for solving massive discrete POSs increase rapidly.

To address the above problems, a multi-objective robust optimal secure operation model for large-scale power grid with multiple B2B VSC systems considering SCC limitation is proposed based on nonlinear AC power flow equations. The main contributions of this paper are threefold.

1) An SCC calculation model for power grid with B2B VSC systems is proposed. The optimal operation modes include TS, BS, UC, and regulation of the power output, terminal voltage of generators, and modulation ratios of B2B VSC systems.

2) To achieve the reliable and efficient solution, the convex relaxation method, including the inscribed N-sided approximation to relax the nonlinear SCC limitation constraint, is proposed to transform the original MINLP model into a mixed-integer convex programming (MICP) model. In addition, an improved checking-adding-checking again-adding again method is proposed to reduce the scale of the proposed multi-objective robust optimization model when the convex relaxation method is applied.

3) A method to directly solve the COS combined with the column-and-constraint generation (C&CG) algorithm is presented to solve the proposed multi-objective robust optimization model, which can improve the computational efficiency and obtain a robust COS with a higher comprehensive optimization degree.

The rest of this paper is organized as follows. An SCC calculation model for power grid with B2B VSC systems is proposed in Section II. The multi-objective robust optimal secure operation model considering the SCC limitation is established in Section III. The convex relaxation method for transforming the original MINLP model into an MICP model to improve the computational efficiency is discussed in Section IV. The solution method is proposed in Section V. Section VI introduces the case studies in an actual large-scale provincial power grid and the modified IEEE 39-bus power grid. Conclusions are presented in Section VII.

II. SCC Calculation Model for Power Grid with B2B VSC Systems

A. Expression of SCC Constraint

The SCC calculation model only considers the most severe three-phase short-circuit faults. After a metallic three-phase short-circuit fault occurs at bus f, the SCC provided by synchronous generators and the injected power source from external power grids, denoted as I_f, is calculated as:

$$I_f = V_{f0}/Z_{ff} \tag{1}$$

There are usually massive RESs in large-scale power grids, and it is necessary to consider the SCC provided by RESs. When a short-circuit fault occurs, the RES containing inverter-based generators can be considered as a constant current source, usually with a preset current value of 1.0 p.u. [21]. According to the superposition theorem, the SCC of a large-scale power grid with RESs is composed of two parts: ① I_f in (1); and ② the SCC provided by equivalent current sources of RESs, denoted as I_{Rfi}, which is expressed as:

$$I_{Rfi} = I_{RE} Z_{fi}/Z_{ff} \tag{2}$$

Compared with I_f, I_{Rfi} is relatively small. The SCC constraint is written as:

$$I_f+\sum_{i\in\Omega_{RE}} I_{Rfi}=V_{f0}/Z_{ff}+\sum_{i\in\Omega_{RE}} I_{RE}Z_{fi}/Z_{ff}\le I_{f\max} \tag{3}$$

In the majority of existing literature, to simplify the computational complexity, the DC power flow model is used to describe the SCC constraint. The power grid is approximately regarded as a purely inductive grid, and the bus voltage is regarded as 1.0 p.u., without considering the influence of RESs on the SCC. However, the DC power flow model has the disadvantage of low accuracy, which may result in the problem of SCC exceeding the secure limit during the actual power grid operation. Therefore, considering AC power flow equations and the influences of synchonous generator output, bus voltage amplitude, line impedance, and RESs on the system SCC, the more accurate SCC constraints are written as:

$$V_{f0}+\sum_{i\in\Omega_{RE}} I_{RE}Z_{fi}\le I_{f\max}Z_{ff} \tag{4}$$

$$Z_{ff}=\sqrt{R_{ff}^2+X_{ff}^2} \tag{5}$$

$$Z_{fi}=\sqrt{R_{fi}^2+X_{fi}^2} \tag{6}$$

To avoid the approximation error of nonlinear terms generated in the inversion calculation of admittance matrix, the form of the product of admittance matrix and impedance matrix is adopted. When a short-circuit fault occurs at bus f, the product of admittance matrix $\boldsymbol{Y}$ and the f^{th} column vector in the impedance matrix $\boldsymbol{Z}_f$ is written as:

$$\boldsymbol{Y}\boldsymbol{Z}_f=\boldsymbol{E}_f \tag{7}$$

B. SCC Calculation for TS, BS, and UC

When TS, BS, and are considered, assuming that all lines and units are in operation in the initial state, the admittance matrix $\boldsymbol{Y}$ can be written as the sum of initial admittance matrix $\boldsymbol{Y}_0$ and increment matrix $\Delta\boldsymbol{Y}$ of TS, BS, and UC, and (7) is rewritten as:

$$(\boldsymbol{Y}_0+\Delta\boldsymbol{Y})\boldsymbol{Z}_f=\boldsymbol{E}_f \tag{8}$$

When the transmission line k (associated with buses i and j) is open, it only affects four elements in the admittance matrix $\boldsymbol{Y}$, i.e., the self-admittances and mutual admittances of buses i and j. Thus, only four elements in the increment matrix of TS $\Delta\boldsymbol{Y}_l$ are non-zero, as expressed in (9), while other elements are all 0.

$$\begin{cases}\Delta Y_{l,ii}=\Delta Y_{l,jj}=-y_{ij}\\ \Delta Y_{l,ij}=\Delta Y_{l,ji}=y_{ij}\end{cases} \tag{9}$$

For the BS, the sectionalization bus is divided into two buses connected with an infinitesimal reactance. Thus, the expression of the increment matrix of BS is consistent with that of TS, as given in (9).

When generator at bus i is shut down, it only affects one element in the admittance matrix $\boldsymbol{Y}$, i.e., the self-admittance of bus i. Thus, only one element in the increment admittance matrix of UC $\Delta\boldsymbol{Y}_g$ is non-zero, as expressed in (10), while other elements are all 0.

$$\Delta Y_g(i,i)=1/x_{gi} \tag{10}$$

Therefore, considering TS, BS, and UC, the impedance vector $\boldsymbol{Z}_f$ can be calculated based on:

$$(\boldsymbol{Y}_0+\varsigma_l\Delta\boldsymbol{Y}_l+\varsigma_g\Delta\boldsymbol{Y}_g)\boldsymbol{Z}_f=\boldsymbol{E}_f \tag{11}$$

C. SCC Calculation for B2B VSC Systems

In an actual large-scale power grid, to limit the SCC level, multiple B2B VSC systems are constructed in the dense-load areas, dividing the large-scale power grid into two small-scale asynchronous power grids, as shown in Fig. 1.

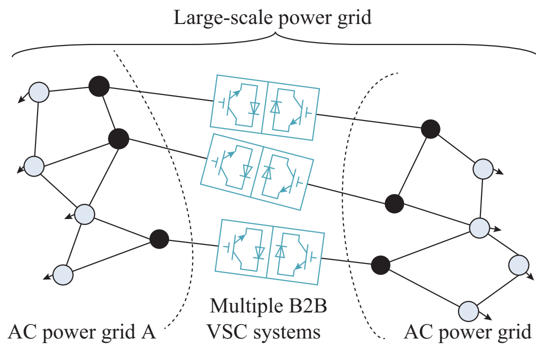

Fig. 1. Structure diagram of a large-scale power grid with multiple B2B VSC systems.

Since the SCC constraints (4)-(6) only need to make the root-mean-square value of the fundamental component of SCC meet the secure limit, the operation model of the B2B VSC system can be described as a steady-state model according to the sinusoidal steady-state circuit theory. The equivalent circuit of a B2B VSC system installed on the AC line i-j' is shown in Fig. 2, and the bus j is added to represent one end of the B2B VSC system.

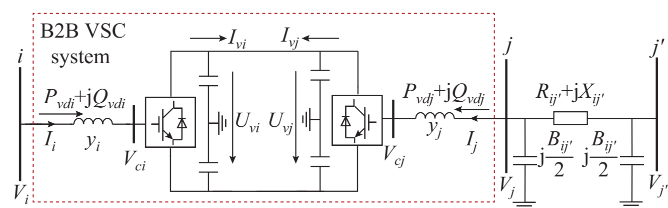

Fig. 2. Equivalent circuit of B2B VSC system installed on AC line i-j'.

The transmission loss and voltage drop of the DC line in the B2B VSC system are ignored because the DC line is very short, i.e., $U_{vi}=U_{vj}$. The relationship between V_{ci} and V_{cj} is shown in (12), and the state variable relationships of buses i and j connecting two ends of the B2B VSC system are shown in (13) and (14) [22].

$$\begin{cases}V_{ci}=\dfrac{\mu_i M_i}{\sqrt{2}}U_{vi}\\ V_{cj}=\dfrac{\mu_j M_j}{\sqrt{2}}U_{vj}\end{cases} \tag{12}$$

$$\begin{cases}I_i=(V_i-V_{ci})y_i\\ I_j=(V_j-V_{cj})y_j\end{cases} \tag{13}$$

$$\begin{cases}P_{vdi}=-P_{vdj}\\ U_{vj}=U_{vi}\\ I_{vj}=-I_{vi}\\ P_{vdi}=V_{ci}I_i\cos\varphi_{ci}\\ P_{vdj}=V_{cj}I_j\cos\varphi_{cj}\end{cases} \tag{14}$$

To limit the SCC level of large-scale power grids, a novel SCC limitation mode using multiple B2B VSC systems to separate a large-scale AC power grid into two asynchronous power grids is proposed. The SCC calculation for B2B VSC system is equivalent to calculating the equivalent admittance of buses i and j connecting two ends of the B2B VSC system, as given in (15)-(19), and the detailed process is shown in Supplementary Material A. Among them, the ratio of the modulation ratios of two VSC stations connected to buses i and j is introduced as $M_{ij}=M_i/M_j$.

$$P_{vdi}^2+Q_{vdi}^2=S_{vdi}^2 \tag{15}$$

$$Y_{v,ii}= I_i/V_i\big|_{V_j=0}=M_{ij}^2 S_{vdi} y_i y_j/(S_{vdi} y_j+M_{ij}^2 S_{vdj} y_i) \tag{16}$$

$$Y_{v,jj}= I_j/V_j\big|_{V_i=0}=M_{ij}^2 S_{vdj} y_i y_j/(S_{vdi} y_j+M_{ij}^2 S_{vdj} y_i) \tag{17}$$

$$Y_{v,ij}= I_i/V_j\big|_{V_i=0}=-M_{ij} S_{vdi} y_i y_j/(S_{vdi} y_j+M_{ij}^2 S_{vdj} y_i) \tag{18}$$

$$Y_{v,ji}= I_j/V_i\big|_{V_j=0}=-M_{ij} S_{vdj} y_i y_j/(S_{vdi} y_j+M_{ij}^2 S_{vdj} y_i) \tag{19}$$

It can be observed that integrating a B2B VSC system into power grid to limit the SCC level is equivalent to connecting an adjustable impedance between buses i and j, and can change the currents I_i and I_j to make them unequal, increase the self-impedance of the short-circuit point, and reduce the SCC level. The above SCC limitation mode can be adjusted by the modulation ratios M_i and M_j, the absorbed active power P_{vdi} and P_{vdj}, and the absorbed reactive power Q_{vdi} and Q_{vdj}. Specifically, when $M_{ij}=1$ and $\cos\varphi_{ci}=\cos\varphi_{cj}$, it can be demonstrated that y_i and y_j are directly connected in series. When M_{ij} tends to be 0 or infinity, the mutual admittances Y_{ij} and Y_{ji} tend to be 0, and the impedance between buses i and j tends to be infinity, which can be demonstrated that the two buses are disconnected but the active power can still be transmitted by the AC line normally. Therefore, integrating multiple B2B VSC systems to separate a large-scale power grid into two asynchronous power grids can effectively reduce the SCC level.

In the increment matrix $\Delta\boldsymbol{Y}_v$, only the four elements associated with self-admittances and mutual admittances are nonzero, as given in (16)-(19), and other elements are all zero. In summary, the calculation of impedance vector $\boldsymbol{Z}_f$ considering the TS, BS, UC, and regulation of modulation ratios of B2B VSC systems can be calculated based on (20).

$$(\boldsymbol{Y}_0+\varsigma_l\Delta\boldsymbol{Y}_l+\varsigma_g\Delta\boldsymbol{Y}_g+\Delta\boldsymbol{Y}_v)\boldsymbol{Z}_f=\boldsymbol{E}_f \tag{20}$$

From (20), the self-impedance Z_{ff} and mutual impedance Z_{fi} in (4) can be changed by TS, BS, UC, and regulation of the modulation ratios. In addition, V_{f0} in (4) can be changed by regulating the power output and terminal voltage of generators. Therefore, these modes can coordinately adjust the SCC level to satisfy the secure limit.

III. Multi-objective Robust Optimal Secure Operation Model

A. Objective Functions

To consider the multiple objectives and the uncertainty of RES output, a multi-objective robust optimal secure operation model of large-scale power grid with multiple B2B VSC systems considering the SCC limitation is established. The objective functions include the total operation cost, total bus voltage deviation, and total power loss of the power grid.

Objective function 1: this objective is to minimize the total operation cost of the power grid, including the switching line cost, generator fuel and shut-down costs, and the power curtailment cost of RESs.

$$\min_{\boldsymbol{x}}\max_{\boldsymbol{v}} f_1=\sum_{k\in\Omega_k} c_k\varsigma_{lk}+\sum_{i\in\Omega_G}[a_{i2}P_{Gi}^2+a_{i1}P_{Gi}+a_{i0}(1-\varsigma_{gi})]+\sum_{i\in\Omega_G} c_{gi}\varsigma_{gi}+\sum_{i\in\Omega_{RE}} c_{wi}(P_{REi\max}-P_{REi}) \tag{21}$$

Objective function 2: this objective is to minimize the total bus voltage deviation of the power grid, aiming to make the load bus voltage closer to the rated value, which contributes to the long-term secure operation of loads.

$$\min_{\boldsymbol{x}}\max_{\boldsymbol{v}} f_2=\sum_{i=1}^{n}(V_i-V_{iN})^2 \tag{22}$$

Objective function 3: this objective is to minimize the total power loss of power grid, aiming to reduce the energy loss and improve the energy utilization efficiency.

$$\min_{\boldsymbol{x}}\max_{\boldsymbol{v}} f_3=\sum_{i\in\Omega_G} P_{Gi}+\sum_{i\in\Omega_{RE}} P_{REi}-\sum_{i\in\Omega_L} P_{Li} \tag{23}$$

According to (21)-(23), the decision variable vector $\boldsymbol{x}$ includes TS, BS, UC, modulation ratios M_i and M_j, and power output and terminal voltage of generators, and the uncertain variable vector $\boldsymbol{v}$ includes $P_{REi\max}$.

B. AC Power Flow Constraints

AC power flow constraints include the power balance equations of AC buses and the power output limit constraints of generators, as given in (24) and (25), respectively.

$$\begin{cases} P_{Gi}+P_{REi}-P_{Li}-P_{vdi}-V_i\sum\limits_{j=1,j\neq i}^{n}V_j(G_{ij}\cos\theta_{ij}+B_{ij}\sin\theta_{ij})=0 \\ Q_{Gi}+Q_{REi}-Q_{Li}-Q_{vdi}-V_i\sum\limits_{j=1,j\neq i}^{n}V_j(G_{ij}\sin\theta_{ij}-B_{ij}\cos\theta_{ij})=0 \end{cases} \tag{24}$$

$$\begin{cases} (1-\varsigma_{gi})P_{Gi\min}\leq P_{Gi}\leq(1-\varsigma_{gi})P_{Gi\max} \\ (1-\varsigma_{gi})Q_{Gi\min}\leq Q_{Gi}\leq(1-\varsigma_{gi})Q_{Gi\max} \end{cases} \tag{25}$$

C. Operation Constraints of B2B VSC System

According to the equivalent circuit model of B2B VSC system, as shown in Fig. 2, its operation constraints are given as:

$$\begin{cases} P_{vdi}=U_{vi}I_{vi} \\ U_{vi}=U_{vj} \\ P_{vdi}=-P_{vdj} \end{cases} \tag{26}$$

$$\begin{cases} P_{vdi}-\dfrac{\mu_i M_i}{\sqrt{2}}V_iU_{vi}y_i\sin\delta_i=0 \\ Q_{vdi}+\dfrac{\mu_i M_i}{\sqrt{2}}V_iU_{vi}y_i\cos\delta_i-V_i^2y_i=0 \end{cases} \tag{27}$$

D. SCC Constraints

The SCC levels of all critical buses are required to be lower than the secure limit. For the three-phase short-circuit fault at one bus, the SCC calculation and limitation constraints are given in (4)-(6), (9)-(10), and (15)-(20).

E. Upper and Lower Limit Constraints of Variables

The upper and lower limit constraints in the proposed multi-objective robust optimization model are given as:

$$\boldsymbol{\phi}_{\min} \le \boldsymbol{\phi} \le \boldsymbol{\phi}_{\max} \tag{28}$$

where $\boldsymbol{\phi} = [V_i, M_i, P_{vdi}, Q_{vdi}, U_{vi}, I_{vi}, P_{REi}, Q_{REi}]$.

To ensure the normal and secure operation of the voltage source converter (VSC) itself, the lower and upper limits of M_i are set to be 0.5 and 1.0, respectively [23], [24].

F. Uncertainty Set Constraints

A box uncertainty set is used to describe the uncertainty of RES output as:

$$(1-\alpha_d)P_{REi,pre} \le P_{REi\max} \le (1+\alpha_u)P_{REi,pre} \tag{29}$$

Therefore, the multi-objective robust optimal secure operation model includes (4)-(6), (9)-(10), and (15)-(29), which is a bi-layer MINLP model. This model will have high computational complexity and low computational efficiency when applied to the large-scale power grid. To achieve the reliable and efficient solution, several convex relaxation methods including the inscribed N-sided approximation are proposed to transform the large-scale MINLP model into an MICP model.

IV. Convex Relaxation for Large-scale MINLP Model

A. Convex Relaxation of AC Power Flow Equations

By introducing variables satisfying (30), the AC power flow constraints in (24) after using second-order cone (SOC) relaxation are transformed into (31) [22].

$$\begin{cases} T_{ij} = V_i V_j \cos\theta_{ij} \\ H_{ij} = V_i V_j \sin\theta_{ij} \\ U_i = V_i^2 \end{cases} \tag{30}$$

$$\begin{cases} P_{Gi} + P_{REi} - P_{Li} - P_{vdi} - U_i G_{ii} - \sum\limits_{j=1, j\ne i}^{n} (T_{ij}G_{ij} + H_{ij}B_{ij}) = 0 \\ Q_{Gi} + Q_{REi} - Q_{Li} - Q_{vdi} + U_i B_{ii} - \sum\limits_{j=1, j\ne i}^{n} (H_{ij}G_{ij} - T_{ij}B_{ij}) = 0 \\ \left\| 2T_{ij} \quad 2H_{ij} \quad U_i - U_j \right\|_2 - (U_i + U_j) \le 0 \\ T_{ij} - T_{ji} = 0 \\ H_{ij} + H_{ji} = 0 \\ \sum\limits_{ij \in \Omega_{ij}} \left(\arctan(H_{ij}^0 / T_{ij}^0) + \dfrac{T_{ij}^0 H_{ij} - H_{ij}^0 T_{ij}}{(T_{ij}^0)^2 + (H_{ij}^0)^2} \right) = 0 \end{cases} \tag{31}$$

B. Convex Relaxation of SCC Calculation Model

1) Convex Relaxation of SCC Constraints

For the SCC constraints (4)-(6), the optimization direction is to maximize Z_{ff} and minimize Z_{fi}. The expression of Z_{fi} in (6) can directly use SOC relaxation, as given in (32), and this relaxation is accurate. However, the expression of Z_{ff} in (5) cannot use SOC relaxation. Substituting (5) into (4) and squaring both sides of the inequality, we can obtain (33).

$$Z_{fi}^2 \ge R_{fi}^2 + X_{fi}^2 \tag{32}$$

$$\left(V_{f0} + \sum_{i \in \Omega_{RE}} I_{REi} Z_{fi} \right)^2 \le I_{f\max}^2 (R_{ff}^2 + X_{ff}^2) \tag{33}$$

Formula (33) is a non-convex quadratic inequality constraint, which is written in a standard form as (34), and its feasible region in the first quadrant is Region 1 in Fig. 3(a), and the relaxed region is Region 2. The commonly-used approximate linearization method for non-convex quadratic inequality constraints is the inscribed quadrilateral approximation, and its expression is expressed as (35). The feasible region of inscribed quadrilateral approximation is Regions 1 and 2 in Fig. 3(a), and the relaxed region is Region 2.

$$x_1^2 + x_2^2 \ge y^2 \quad y > 0 \tag{34}$$

$$\pm x_1 \pm x_2 \ge y \quad y > 0 \tag{35}$$

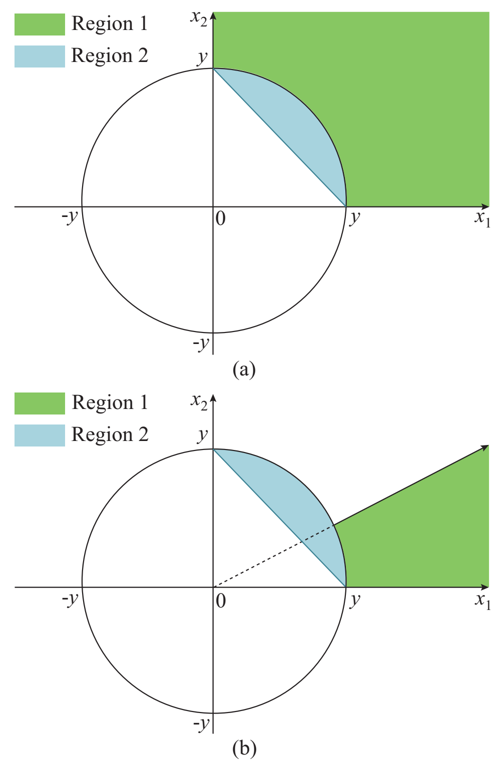

Fig. 3. Feasible and relaxed regions of original non-convex constraint (34) and inscribed quadrilateral approximation. (a) Original non-convex constraint (34). (b) Inscribed quadrilateral approximation.

For the actual high-voltage power grid, the reactance X_{ff} will be much greater than the resistance R_{ff}, that is, the effective feasible region of the original non-convex constraint (34) will be concentrated in the area close to the abscissa axis (taking X_{ff} as x_1 and R_{ff} as x_2), as shown in Fig. 3(b).

An inscribed N-sided approximation method is proposed to reduce the relaxed region and improve the approximation accuracy, where N is a large positive number, and only one side of the N-sided shape close to the abscissa axis is required to approximate the original non-convex constraint (34), as shown in Fig. 4. The feasible region of inscribed N-sided approximation method is Regions 1 and 3, and the relaxed region is Region 3. It can be observed that the relaxed region of the inscribed N-sided approximation method is significantly reduced compared with that of the inscribed quadrilateral approximation. According to $X_{ff} >> R_{ff}$, we make $x_1 = kx_2$, $k = 1/\tan(2\pi/N)$, and $N > 8$. For example, when $N = 32$, $k = 5.027$. Then, the coordinate values of the intersection point h in Fig. 4 is calculated as $(k/\sqrt{k^2+1}\cdot y, 1/\sqrt{k^2+1}\cdot y)$, and the inscribed N-sided approximation method is expressed as (36).

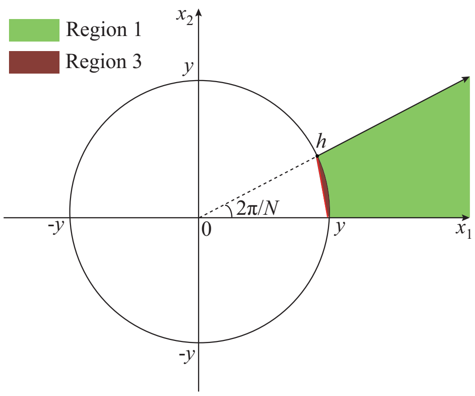

Fig. 4. Feasible and relaxed regions of inscribed N-sided approximation method.

$$\begin{cases} \pm x_1 \pm (\sqrt{k^2+1} - k)x_2 \geq y \quad y > 0 \\ \pm x_1 \geq \pm k x_2 \end{cases} \tag{36}$$

The binary variables R_{ff+}, R_{ff-}, X_{ff+}, and X_{ff-} are introduced to indicate the positive or negative sign of R_{ff} and X_{ff}, and the SCC constraint (33) is linearized as:

$$\begin{cases} V_{f0} + \sum\limits_{i \in \Omega_{RE}} I_{REi} Z_{fi} \leq I_{f\max}[X'_{ff} + (\sqrt{k^2+1} - k)R'_{ff}] \\ X'_{ff} \geq kR'_{ff} \\ R_{ff} = R_{ff+} + R_{ff-} \\ X_{ff} = X_{ff+} + X_{ff-} \\ R'_{ff} = R_{ff+} - R_{ff-} \\ X'_{ff} = X_{ff+} - X_{ff-} \\ 0 \leq R_{ff+} \leq \varsigma_R M \\ -(1-\varsigma_R)M \leq R_{ff-} \leq 0 \\ 0 \leq X_{ff+} \leq \varsigma_X M \\ -(1-\varsigma_X)M \leq X_{ff-} \leq 0 \end{cases} \tag{37}$$

In addition, for the non-convex quadratic equality $U_f = V_{f0}^2$ introduced by the SOC relaxation of AC power flow equations, the convex envelope relaxation method is used to transform it into convex inequality constraints as [25]:

$$\begin{cases} V_{f0}^2 - U_f \leq 0 \\ U_f - V_{f\min}^2 - (V_{f\max} + V_{f\min})(V_{f0} - V_{f\min}) \leq 0 \end{cases} \tag{38}$$

2) Convex Relaxation of SCC Calculation Constraints

The SCC calculation constraints of a power grid with B2B VSC systems in (15)-(20) are all non-convex. For (15), the SOC relaxation method can be directly used as:

$$P_{vdi}^2 + Q_{vdi}^2 \leq S_{vdi}^2 \tag{39}$$

For the multiplication terms of binary variables and continuous variables in (20), $\boldsymbol{W}_l = \varsigma_l \boldsymbol{Z}_f$ and $\boldsymbol{W}_g = \varsigma_g \boldsymbol{Z}_f$ are introduced, and then they can be linearized by big-M method as:

$$\begin{cases} -M\boldsymbol{\varsigma}_l \leq \boldsymbol{W}_k \leq M\boldsymbol{\varsigma}_l \\ -M(\boldsymbol{1} - \varsigma_l) + \boldsymbol{Z}_f \leq \boldsymbol{W}_l \leq M(\boldsymbol{1} - \varsigma_l) + \boldsymbol{Z}_f \\ -M\boldsymbol{\varsigma}_g \leq \boldsymbol{W}_g \leq M\boldsymbol{\varsigma}_g \\ -M(\boldsymbol{1} - \varsigma_g) + \boldsymbol{Z}_f \leq \boldsymbol{W}_g \leq M(\boldsymbol{1} - \varsigma_g) + \boldsymbol{Z}_f \end{cases} \tag{40}$$

For the multiplication term $\Delta \boldsymbol{Y}_v \boldsymbol{Z}_f$ in (20), only four non-zero elements $Y_{v,ii}$, $Y_{v,ij}$, $Y_{v,ji}$, and $Y_{v,jj}$ in $\Delta \boldsymbol{Y}_v$ are multiplied by the corresponding elements in $\boldsymbol{Z}_f$. Four variables are introduced as:

$$\begin{cases} W_{v,ii} = Y_{v,ii} Z_{if} \\ W_{v,ij} = Y_{v,ij} Z_{jf} \\ W_{v,ji} = Y_{v,ji} Z_{if} \\ W_{v,jj} = Y_{v,jj} Z_{jf} \end{cases} \tag{41}$$

Taking $W_{v,ii} = Y_{v,ii} Z_{if}$ for convex relaxation derivation as an example, the obtained results are shown in (42) and (43), and the detailed derivation process is shown in Supplement Material A.

$$\begin{cases} M_{ij} = \sum\limits_b \xi_{ijb} M_{ijb0} \\ \sum\limits_b \xi_{ijb} = 1 \end{cases} \tag{42}$$

$$\begin{cases} (S_{vdi} y_j + W_{MSij} y_i + W_{v,ii})^2 + (S_{vdi} y_i y_j - Z_{if})^2 \leq H_{v,ii}^2 \\ (S_{vdi} y_i y_j + Z_{if})^2 + (S_{vdi} y_j + W_{MSij} y_i - W_{v,ii})^2 \leq H_{v,ii}^2 \end{cases} \tag{43}$$

where $W_{MSij} = M_{ij}^2 S_{vdj}$ is an introduced intermediate variable.

The other three equations in (41) are similarly executed by convex relaxation method, and then $\Delta \boldsymbol{Y}_v \boldsymbol{Z}_f$ can be expressed in the linear form as:

$$\Delta \boldsymbol{Y}_v \boldsymbol{Z}_f = [0 \quad \dots \quad W_{v,ii} + W_{v,ij} \quad \dots \quad W_{v,ji} + W_{v,jj} \quad \dots \quad 0]^{\mathrm{T}} \tag{44}$$

Therefore, the non-convex constraints (15)-(20) are transformed into the convex constraints (39), (40), and (42)-(44).

C. Convex Relaxation of Operation Constraints for B2B VSC System

For the operation constraints of B2B VSC system, by introducing $\bar{I}_{vi} = I_{vi}^2$ and $\bar{U}_{vi} = U_{vi}^2$, (26) is transformed into (45) after SOC relaxation; by introducing $K_{vi} = M_i V_i U_{vi} \sin\delta_i$, $L_{vi} = M_i V_i U_{vi} \cos\delta_i$, $\bar{M}_i = M_i^2$, and $\Psi_i = \bar{M}_i \bar{U}_{vi}$, (27) is transformed into (46) by using SOC and convex envelope relaxation methods.

$$\begin{cases} \left\| 2P_{vdi} \quad \bar{I}_{vi} - \bar{U}_{vi} \right\|_2 - (\bar{I}_{vi} + \bar{U}_{vi}) \leq 0 \\ \bar{U}_{vi} = \bar{U}_{vj} \\ P_{vdi} = -P_{vdj} \end{cases} \tag{45}$$

$$\begin{cases} P_{vdi} - \dfrac{\mu_i}{\sqrt{2}} y_i K_{vi} = 0 \\ Q_{vdi} + \dfrac{\mu_i}{\sqrt{2}} y_i L_{vi} - \bar{U}_{vi} y_i = 0 \\ \left\| 2K_{vi} \quad 2L_{vi} \quad \Psi_i - \bar{U}_{vi} y_i \right\|_2 \le \Psi_i + \bar{U}_{vi} y_i \\ \bar{U}_{vi\min} \bar{M}_i + \bar{M}_{i\min} \bar{U}_{vi} - \bar{U}_{vi\min} \bar{M}_{i\min} - \Psi_i \le 0 \\ \bar{U}_{vi\max} \bar{M}_i + \bar{M}_{i\max} \bar{U}_{vi} - \bar{U}_{vi\max} \bar{M}_{i\max} - \Psi_i \le 0 \\ \Psi_i - \bar{U}_{vi\min} \bar{M}_i - \bar{M}_{i\max} \bar{U}_{vi} + \bar{U}_{vi\min} \bar{M}_{i\max} \le 0 \\ \Psi_i - \bar{U}_{vi\max} \bar{M}_i - \bar{M}_{i\min} \bar{U}_{vi} + \bar{U}_{vi\max} \bar{M}_{i\min} \le 0 \end{cases} \tag{46}$$

For the SOC constraints in (31), (32), (39), (43), (45), and (46), the successive inscribed polygon method proposed in [22] can be used to tighten the relaxation gap to meet the requirements of computational accuracy. Therefore, after the convex relaxation, the transformed MICP model includes (9), (10), (21)-(23), (25), (28), (29), (31), (32), (37)-(40), and (42)-(46). The mature commercial solver GUROBI is used to efficiently solve this MICP model for the optimal operation of large-scale power grids.

V. Solution Method

A. Method to Directly Solve COS Combined with C&CG Algorithm

A multi-objective robust optimization model with P optimization objectives is written in the compact form as:

$$\begin{cases} \min\limits_{x} \max\limits_{v} \left(f_1(\boldsymbol{x},\boldsymbol{v}), f_2(\boldsymbol{x},\boldsymbol{v}), ..., f_P(\boldsymbol{x},\boldsymbol{v})\right) \\ \text{s.t. } \boldsymbol{x} \in X, \boldsymbol{v} \in \Omega \end{cases} \tag{47}$$

The commonly-used solution method for multi-objective robust optimization model is first to solve massive POSs to form the POS set, and then select a COS as the decision result from the POS set. However, obtaining the POS set requires massive computational time. In order to improve the computational efficiency considering various objectives comprehensively and ensure the robustness of the obtained optimal operation mode, a method to directly solve the COS combined with the C&CG algorithm is proposed to solve the multi-objective robust optimization model.

The objective function is to minimize the normalized distance between the multi-objective optimization solutions and the utopia point d_+, as well as to maximize the normalized distance between the multi-objective optimization solution and the nadir point d_-, as expressed in (48).

$$\begin{cases} \min\limits_{x} \max\limits_{v} \Delta d^2 = d_+^2 - d_-^2 \\ \text{s.t. } d_{p+} = \dfrac{f_p(\boldsymbol{x},\boldsymbol{v}) - f_p(x^{p*})}{f_{p\max} - f_p(x^{p*})} \quad p = 1,2,...,P \\ \qquad d_{p-} = \dfrac{f_{p\max} - f_p(\boldsymbol{x},\boldsymbol{v})}{f_{p\max} - f_p(x^{p*})} \quad p = 1,2,...,P \\ \qquad \boldsymbol{x} \in X, \ \boldsymbol{v} \in \Omega \end{cases} \tag{48}$$

where x^{p*} and $f_{p\max}$ are explained at the end of this subsection; and the relationship between d_+, d_- and d_{p+}, d_{p-} is shown in (50).

The schematic diagram for directly solving the COS of bi-objective robust optimization model is shown in Fig. 5.

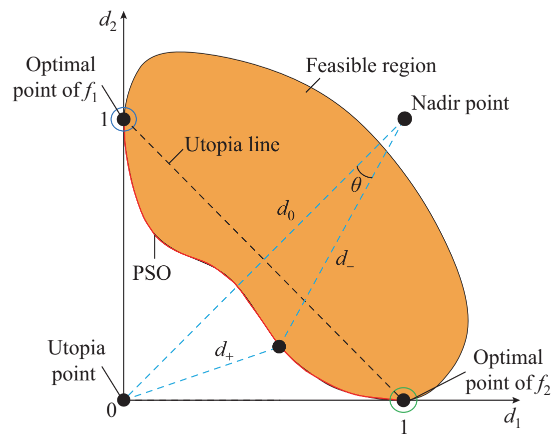

Fig. 5. Schematic diagram for directly solving COS of bi-objective robust optimization model.

According to the cosine theorem, inner product formula of vectors, and Fig. 5, the objective function in (48) can be derived into a linear objective function as (49), and (48) can be re-written as (50). For the optimization model in (50), the constraints include (9)-(10), (21)-(23), (25), (28), (29), (31), (32), (37)-(40), (42)-(46). Thus, (50) is also a bi-layer MICP model.

$$d_+^2 - d_-^2 = d_0^2 - 2d_0 d_- \cos\theta = d_0^2 - 2\boldsymbol{d}_0 \cdot \boldsymbol{d}_- = d_0^2 - 2(1 - d_{1+} + 1 - d_{2+} + ... + 1 - d_{P+}) = d_0^2 - 2(d_{1-} + d_{2-} + ... + d_{P-}) \tag{49}$$

$$\begin{cases} \min\limits_{x} \max\limits_{v} \Delta d^2 = d_0^2 - 2(d_{1-} + d_{2-} + ... + d_{P-}) \\ \text{s.t. } d_{p-} = \dfrac{f_{p\max} - f_p(\boldsymbol{x},\boldsymbol{v})}{f_{p\max} - f_p(x^{p*})} \quad p = 1,2,...,P \\ \qquad \boldsymbol{x} \in X, \boldsymbol{v} \in \Omega \end{cases} \tag{50}$$

where $\boldsymbol{d}_0 = [1, 1, ..., 1]$; and $\boldsymbol{d}_- = [1 - d_{1+}, 1 - d_{2+}, ..., 1 - d_{P+}]$.

In summary, for a multi-objective robust optimization model with P optimization objectives as (47), the calculation steps of obtaining the COS are as follows. Firstly, by using the C&CG algorithm, the single-objective robust optimization model with each objective $f_p(\boldsymbol{x},\boldsymbol{v})$ is solved, and each single-objective optimization solution x^{p*} is obtained, then the $P \times P$ payment matrix $\boldsymbol{Pay}$ in (51), utopia point, and nadir point are obtained. In addition, the maximum value of the p^{th} column of the payment matrix is recorded as $f_{p\max}$. Then, by using the C&CG algorithm, the two-layer optimization model in (50) is directly solved to obtain a COS without solving massive POSs. By using the C&CG algorithm, the two-layer optimization model in (50) is decomposed into the main problem and sub-problem for alternating iterative solution [26]. The constraints of the main problem include (9), (10), (25), (28), (31), (32), (37)-(40), (42)-(46), and (50), and the constraints of the sub-problem include (25), (28), (29), (31), (45), (46), and (50).

$$\boldsymbol{Pay} = \begin{bmatrix} f_1(x^{1*}) & f_2(x^{1*}) & \dots & f_P(x^{1*}) \\ f_1(x^{2*}) & f_2(x^{2*}) & \dots & f_P(x^{2*}) \\ \vdots & \vdots & & \vdots \\ f_1(x^{P*}) & f_2(x^{P*}) & \dots & f_P(x^{P*}) \end{bmatrix} \tag{51}$$

B. Improved Checking-Adding-Checking Again-Adding Again Method for Solving SCC-constrained Optimization Model

When the proposed multi-objective robust optimization model is applied in a large-scale power grid with thousands of buses, the dimension of the $\boldsymbol{Z}_f$ calculation equation (20) is $n_c \times n$ when considering the SCC constraints of three-phase short-circuit faults of all critical buses at the same time, which will be more than millions of equations, resulting in the great complexity. However, it is noted that the SCC levels of most short-circuit faults are not exceeding the secure limit. Hence, most of the SCC constraints are inactive. Similar to the solution method for the optimal generation dispatch problem considering the network security constraints for large-scale power grids in [27], the while-loop scheme of checking-adding-checking again-adding again method is used to address the above problems.

The existing checking-adding-checking again-adding-again method usually requires many iterations for obtaining the optimal solution, resulting in low computational efficiency. Hence, an improved checking-adding-checking again-adding again method is proposed, and the while-loop scheme is as follows. First of all, a single-objective robust optimization model without SCC constraints is solved by C&CG algorithm and a solution is obtained. Then, the SCC constraints exceeding the secure limit or with the distance margin less than α to the secure limit in the previous iteration will be added in the coming iteration. The procedure is repeated until an optimal solution that meets all SCC constraints is obtained. The flowchart of the while-loop scheme and the method to directly solve the COS is shown in Fig. 6. Specially, when the margin $\alpha = 0$, the improved checking-adding-checking again-adding again method is consistent with the existing method in [27]. With this improved method, each iteration only contains a limited number of SCC constraints, which can obtain the optimal secure operation results that can meet all SCC constraints with fewer iteration and higher computational efficiency.

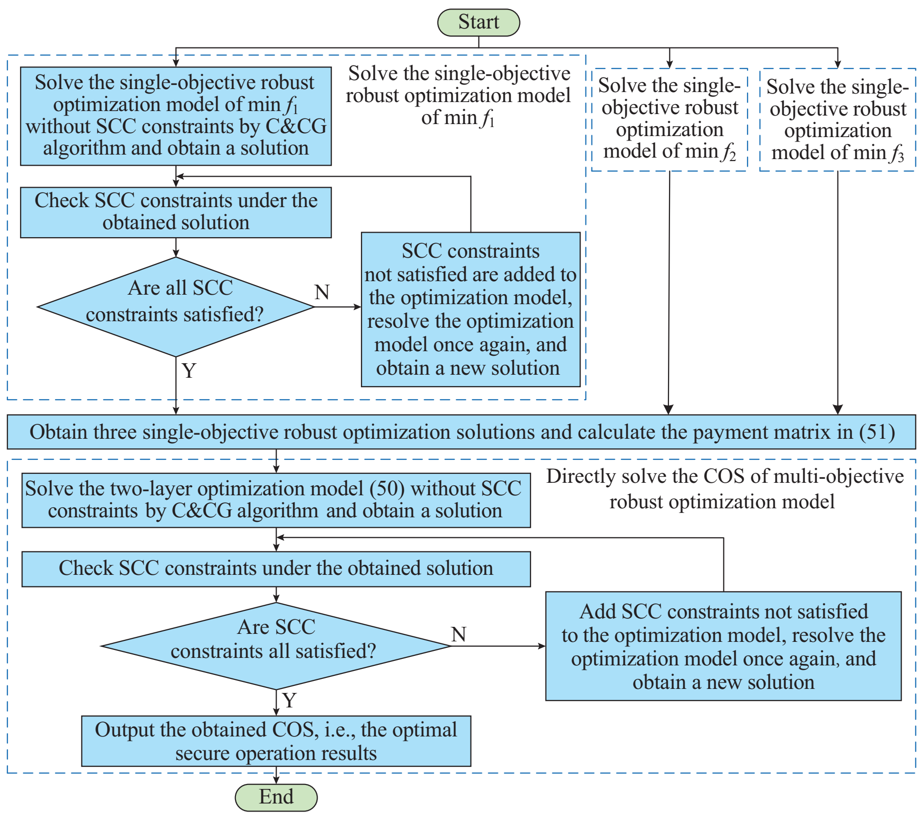

Fig. 6. Flowchart of while-loop scheme and method to directly solve COS.

VI. Case Study

The effectiveness of the proposed solution method is demonstrated by the case studies with an actual large-scale provincial power grid and the modified IEEE 39-bus power grid. The used computer is a PC with an 11$^{\text{th}}$ Gen 2.50 GHz Intel$^{(\text{R})}$ Core $^{(\text{TM})}$ i7-11700 and 32 GB of RAM. The computing platform used in the optimization calculation is GAMS win64 42.2.0.

A. Actual Large-scale Provincial Power Grid

The Guangdong power grid in China is taken as the case, which includes 4407 buses, 5803 branches, 310 synchronous generators, 12 wind farms, 9 photovoltaic stations, and 3 B2B VSC systems, namely the southern channel located at SY-DF line (500 kV), the middle channel located at ZC-SD line (500 kV), and the northern channel located at CX-LM line (500 kV). The Guangdong power grid is separated into two asynchronous power grids interconnected through these three B2B VSC systems, as shown in Fig. 7. The total load power is 103.19 GW, the total installed capacities of wind farms and photovoltaic stations are 8.55 and 2.20 GW, respectively, and the penetration rate of renewable energy is 10.4%. The parameters of three B2B VSC systems are the same, with the rated voltage as ±500 kV, rated capacity as 3200 MVA, and converter reactance as 0.055 Ω. The subtransient reactance of each synchronous generator is basically between 0.18 p.u. and 0.26 p.u.. The parameters of the proposed multi-objective robust optimization model are listed in Table I. Among them, due to different breaking capacities of the circuit breakers installed on transmission lines with different voltage levels, $I_{f\max}$ values for 500 kV and 220 kV buses are 63 kA and 50 kA, respectively.

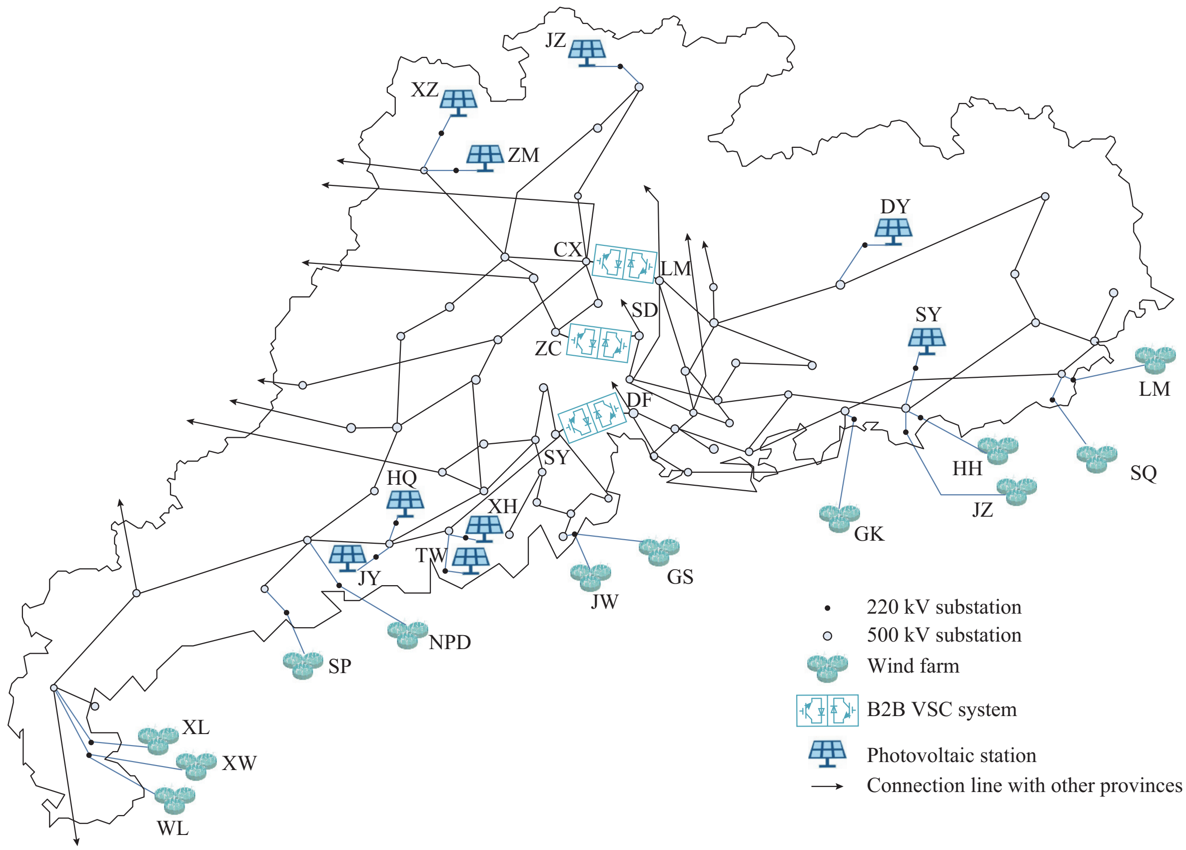

Fig. 7. Basic structure diagram of Guangdong power grid.

TABLE I
PARAMETERS OF PROPOSED MULTI-OBJECTIVE ROBUST OPTIMIZATION MODEL

c_k (¥)	c_{gi} (¥)	c_{wi} (¥/MW)	α (%)	α_d	α_u	N
6×10^4	3×10^4	1000	10	0.25	0.25	32

The SCCs of three-phase short-circuit faults at all 500 kV and 220 kV buses obtained by solving the optimization models without SCC constraints is shown in Fig. 8. Among them, the SCC levels of 12 buses exceed the upper limit, including eight 500 kV buses and four 220 kV buses, which will result in the insecure operation of the system. Thus, these SCC constraints should be added in the proposed multi-objective robust optimization model of power grids. For these faults of 12 buses, the SCCs provided by synchronous generators and RESs are shown in Table II. The proportion of SCC provided by RESs is about 3.5%-5.6% with the penetration rate of renewable energy being 10.4%. When there are more RESs are penetrated into the power grid in the future, the proportion of SCC provided by RESs will be higher. Therefore, for a power grid with high penetration of RESs, neglecting the SCC provided by RESs will result in the unsecure operation of the power grid.

1) Analysis of Optimal Operation Result

The three single-objective robust optimization models are solved, and the optimal operation results with and without B2B VSC systems are shown in Table III. Without B2B VSC system, only the TS, BS, UC, and regulation of the power output and terminal voltage of generators are used to limit SCC. It can be observed from Table III that, the model with B2B VSC system can adjust the modulation ratios, absorbed active and reactive power of the VSC stations, and cooperate with the conventional SCC limitation modes, which can reduce the SCC level to meet the secure limit, and reduce the numbers of shut-down generators or disconnection lines, being beneficial to the secure operation and reliable power supply. Therefore, the above results indicate that using multiple B2B VSC systems to separate this large-scale power grid into two asynchronous power grids and regulating the modulation ratios of these B2B VSC systems have obvious effect on limiting the SCC level and improving the secure and economic operation of the power grid.

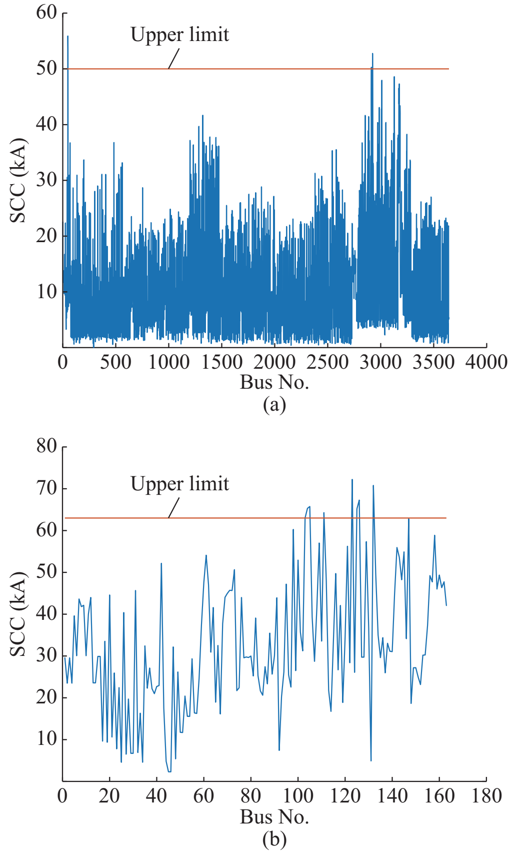

Fig. 8. SCCs of three-phase short-circuit faults at all 500 kV and 220 kV buses obtained by solving optimization model without SCC constraints. (a) 500 kV buses. (b) 220 kV buses.

TABLE II
SCCs Provided by Synchronous Generators and RESs

Rated voltage (kV)	Fault bus	SCC (kA)		
		Total	Synchronous generator	RES
500	GF	63.02	60.50	2.52
	GS	65.31	62.06	3.25
	GA	65.75	62.73	3.02
	JL	64.29	61.40	2.89
	SY	72.23	68.17	4.06
	SD	65.17	62.87	2.30
	WS	67.29	63.68	3.61
	XS	70.80	67.25	3.55
220	XX	55.89	53.33	2.56
	ZN	53.55	50.97	2.58
	JY	50.28	48.33	1.95
	HZ	52.77	49.89	2.88

According to the three single-objective optimization solutions, the payment matrix can be obtained, and then the method to directly solve the two-layer optimization model in (50) is used to obtain the robust COS, which is shown in Table IV. In addition, the SCCs of three-phase short-circuit faults at all 500 kV and 220 kV buses corresponding to the obtained robust COS are shown in Fig. 9.

TABLE III
Results of Three Single-objective Robust Optimization Models

Objective	Model	Optimal operation result	Objective value
min f_1	With B2B VSC	Generator YA1 is shut-down	¥34127300
	Without B2B VSC	Generator YA1 is shut-down Generator YA2 is shut-down Generator SS5 is shut-down Line DL-WY is open Line JM-XJ is open	¥34771100
min f_2	With B2B VSC	Generator ZJ2 is shut-down Line JM-XJ is open	4.5543 p.u.
	Without B2B VSC	Generator ZJ2 is shut-down Generator ZJ4 is shut-down Generator LA1 is shut-down Line DL-WY is open Line JM-XJ is open Line LA-SZ is open	4.7106 p.u.
min f_3	With B2B VSC	Line JM-XJ is open	2738.01 MW
	Without B2B VSC	Generator JH3 is shut-down Generator PH1 is shut-down Line DL-WY is open Line JM-XJ is open Line LA-RJ is open	2826.68 MW

TABLE IV
Results of Obtained Robust COS and Three Single-objective Optimization Solutions

Objective	f_1 value (¥)	f_2 value (p.u.)	f_3 value (MW)	d_+	d_-
min f_1	34127300	9.2591	3012.94	0.987	1.294
min f_2	36714600	4.5543	3470.16	1.414	1.000
min f_3	35217300	10.6259	2738.01	1.085	1.155
Robust COS	34841000	5.8203	2916.20	0.602	1.381

The optimized adjustment results for modulation ratio of B2B VSC systems, and the power output and terminal voltage of some generators with the obtained robust COS is shown in Table V and Table VI, respectively. It can be observed that the SCCs of all buses are lower than the upper limit by adjusting TS, BS, UC, modulation ratio, and power output and terminal voltage of generators, which indicates that the optimal operation results obtained by the proposed solution method can satisfy all SCC constraints. Compared with the three single-objective robust optimization solutions, the obtained robust COS has the smallest distance from the utopia point, and the largest distance from the nadir point. Hence, it has the highest comprehensive optimization degree.

2) Analysis of Accuracy of Convex Relaxation

The results before and after convex relaxation are compared in Table VII. Models 1-3 are detailed as follows.

1) Model 1: the MICP model using inscribed N-sided approximation method with different N values (N=16, 32, 48).

2) Model 2: the MICP model using inscribed quadrilateral approximation method.

3) Model 3: the original MINLP model.

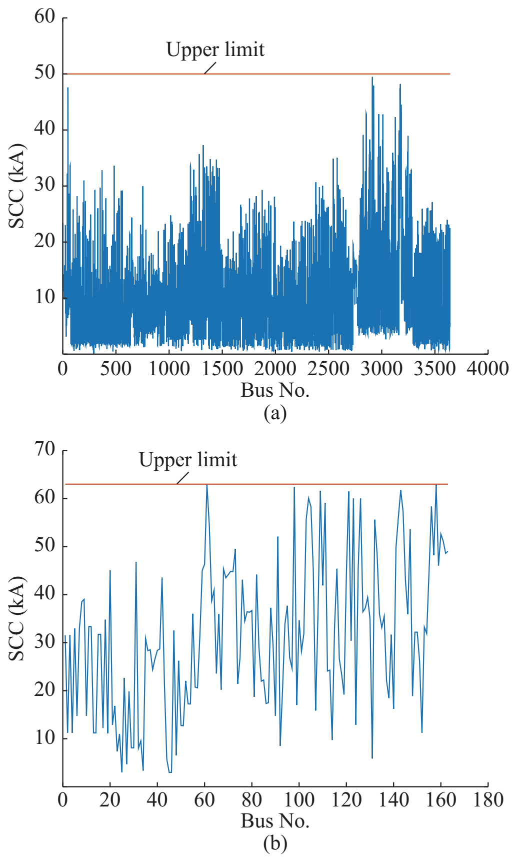

Fig. 9. SCCs of three-phase short-circuit faults at all 500 kV and 220 kV buses corresponding to robust COS. (a) 500 kV buses. (b) 220 kV buses.

TABLE V
ADJUSTMENT RESULTS FOR MODULATION RATIO OF B2B VSC SYSTEMS

Condition	M_i of B2B VSC system at various buses					
	SY	DF	ZC	SD	CX	LM
Before optimization	1.00	1.00	1.00	1.00	1.00	1.00
With robust COS	0.64	0.95	0.50	1.00	0.72	0.89

It can be observed that compared with the results of Model 2, the maximum relaxation gap of Model 1 is reduced by several orders of magnitude, effectively improving the accuracy of convex relaxation for non-convex quadratic inequality constraint (34). Moreover, Model 1 can still greatly improve the computational efficiency compared with Model 3 in terms of the required CPU time. As N increases, the relaxation gap of Model 1 decreases. However, as N increases, the feasible region of (X_{ff}, R_{ff}) constrained by the relaxed SCC constraint (33) will decrease, resulting in higher obtained objective values and lower optimization degrees. Therefore, a suitable N value is required and $N=32$ is selected for the later calculation.

3) Validity Analysis of Improved Checking-Adding-Checking Again-Adding Again Method

In order to verify the effectiveness of the improved checking-adding-checking again-adding-again method, the comparative results under different given margins α are shown in Table VIII. It can be observed that under different α values, the obtained optimal solutions to each single-objective robust optimization model are the same because they must satisfy the requirement that the SCCs of short-circuit faults at all buses are below the upper limit, and the satisfied constraints are consistent. When the margin α increases, more SCC constraints of bus faults are added in each iteration, and the required CPU time for each iteration will increase, but the required iteration number of the while-loop scheme will decrease. When the margin $\alpha \geq 10\%$, the required iteration number reaches the minimum value of 1. Therefore, the total CPU time will decrease first and then increase as the margin α increases. Compared with the existing checking-adding-checking again-adding again method ($\alpha=0$), a suitable margin value ($\alpha=10\%$) can reduce the CPU time by about 60%-70%.

4) Robustness Analysis

To verify the robustness of the optimal operation mode corresponding to the obtained robust COS, the comparative results of solving the proposed multi-objective robust optimization model and the multi-objective deterministic optimization model are shown in Table IX.

The multi-objective deterministic optimization model makes decisions based on the predicted values of RES output. The three objective values of the proposed multi-objective robust optimization model are bigger, but they can satisfy all SCC constraints in the worst scenario of the uncertain RES output.

However, for the multi-objective deterministic optimization model, the SCCs of three 500 kV bus faults and two 220 kV bus faults exceed the upper limit in the worst scenario of the uncertain RES output, as shown in Fig. 10, which will result in the insecure operation of the power grid. Therefore, the optimal operation mode obtained by the proposed multi-objective robust optimization model can ensure the secure operation of power grid under the uncertain fluctuations of RES output.

TABLE VI
POWER OUTPUT AND TERMINAL VOLTAGE OF GENERATORS

Condition	Power output (MW)					Terminal voltage (p.u.)				
	Generator YX1	Generator TS1	Generator WS2	Generator LY2	Generator QK1	Generator YX1	Generator TS1	Generator WS2	Generator LY2	Generator QK1
Before optimization	36.0	28.0	47.0	30.0	15.0	1.020	1.010	1.020	1.000	1.000
With robust COS	33.6	29.4	44.5	33.0	16.5	1.006	1.021	1.015	1.022	1.009

TABLE VII
COMPARATIVE RESULTS BEFORE AND AFTER CONVEX RELAXATION

Objective	Model	Objective value	The maximum relaxation gap	CPU time (s)
min f_1	Model 1 (N=16)	¥33748300	2.24×10^{-3}	1466.1
	Model 1 (N=32)	¥34127300	9.71×10^{-4}	1512.9
	Model 1 (N=48)	¥35085200	4.53×10^{-4}	1710.7
	Model 2	¥33291400	6.83×10^{-2}	1636.3
	Model 3	¥35016000		31127.4
min f_2	Model 1 (N=16)	4.4601 p.u.	5.83×10^{-3}	1475.0
	Model 1 (N=32)	4.5543 p.u.	2.55×10^{-3}	1429.2
	Model 1 (N=48)	4.7216 p.u.	1.46×10^{-3}	1323.4
	Model 2	4.3085 p.u.	1.30×10^{-1}	1392.0
	Model 3	4.7452 p.u.		30934.5
min f_3	Model 1 (N=16)	2699.50 MW	3.55×10^{-3}	1300.9
	Model 1 (N=32)	2738.01 MW	1.61×10^{-3}	1255.8
	Model 1 (N=48)	2796.82 MW	8.87×10^{-4}	1573.3
	Model 2	2644.66 MW	8.28×10^{-2}	1309.5
	Model 3	2829.35 MW		26234.1
Robust COS	Model 1 (N=16)	¥34463800 5.7344 p.u. 2880.91 MW	6.30×10^{-3}	1888.2
	Model 1 (N=32)	¥34841000 5.8203 p.u. 2916.20 MW	2.85×10^{-3}	1725.4
	Model 1 (N=48)	¥35774600 6.0095 p.u. 2972.32 MW	1.71×10^{-3}	1790.3
	Model 2	¥33816200 5.5783 p.u. 2815.95 MW	1.46×10^{-1}	1660.5
	Model 3	¥35734700 6.0354 p.u. 003.19 MW		35949.7

TABLE VIII
COMPARATIVE RESULTS OF IMPROVED CHECKING-ADDING-CHECKING AGAIN-ADDING AGAIN METHOD UNDER DIFFERENT MARGINS α

Objective	α (%)	Objective value	Iteration number of while-loop scheme	CPU time (s)
min f_1	0	¥34127300	3	3371.8
	5	¥34127300	2	2447.9
	10	¥34127300	1	1512.9
	15	¥34127300	1	1890.1
min f_2	0	4.4543 p.u.	4	3889.3
	5	4.4543 p.u.	2	2253.0
	10	4.4543 p.u.	1	1429.2
	15	4.4543 p.u.	1	1741.4
min f_3	0	2738.01 MW	3	2924.1
	5	2738.01 MW	2	2101.5
	10	2738.01 MW	1	1255.8
	15	2738.01 MW	1	1688.9

5) Comparison of Different Multi-objective Optimization Models Considering Uncertainties of Renewable Energy

For various multi-objective optimization models considering the uncertainties of RES output, the comparative results of the proposed multi-objective robust optimization model, the commonly-used multi-objective scenario-based stochastic optimization model [14], and multi-objective adaptive robust optimization model [17] are shown in Table X.

TABLE IX
ROBUSTNESS ANALYSIS OF OPTIMAL OPERATION MODE OF COS

Model	f_1 (¥)	f_2 (p.u.)	f_3 (MW)	Number of bus faults with SCC exceeding limit
Multi-objective deterministic optimization model	34841000	5.8203	2916.20	0
Proposed multi-objective robust optimization model	33930400	5.7099	2831.26	5

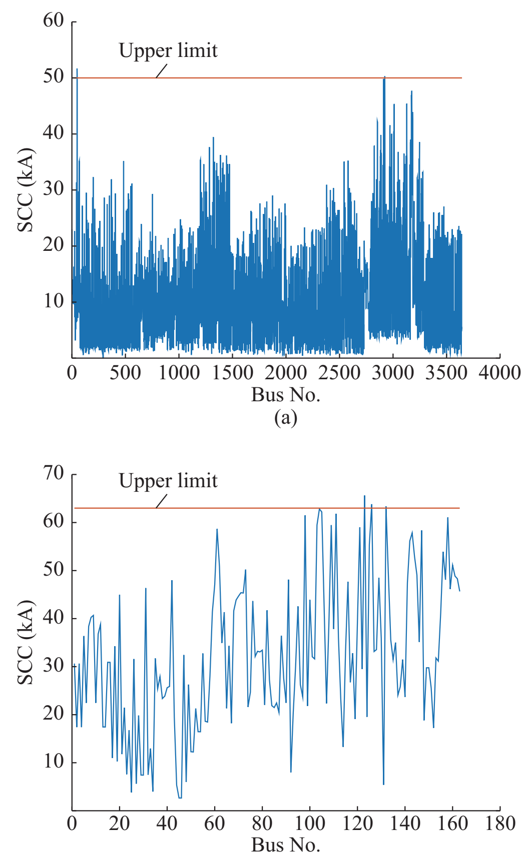

Fig. 10. SCCs of three-phase short-circuit faults at all 500 kV and 220 kV buses by solving multi-objective deterministic optimization model. (a) 500 kV buses. (b) 220 kV buses.

The multi-objective scenario-based stochastic optimization model adopts 10 and 20 stochastic scenarios to reflect the uncertainty of RES output. The uncertainty budgets are set as 0.8 and 1.2 for the RES output in the multi-objective adaptive robust optimization model [17]. It can be observed that compared with the results of multi-objective scenario-based stochastic optimization model, the proposed multi-objective robust optimization model has much higher computational efficiency. As the number of scenarios increases, each objective value of multi-objective scenario-based stochastic optimization model becomes closer to that of the proposed multi-objective robust optimization model. The multi-objective adaptive robust optimization model can reduce the conservatism of the robust optimization results, and each objective value of the optimal solution is lower than that of the proposed multi-objective robust optimization model, but the robustness and security are worse and the CPU time is longer. Therefore, both the proposed multi-objective robust optimization model and multi-objective adaptive robust optimization model can be used to solve the optimal secure operation problem considering the uncertainties of RES output, depending on the actual engineering requirements of the conservatism and robustness of the obtained optimal secure operation mode.

TABLE X
COMPARATIVE RESULTS UNDER VARIOUS MULTI-OBJECTIVE OPTIMIZATION MODELS CONSIDERING UNCERTAINTIES OF RES OUTPUT

Model	f_1 (¥)	f_2 (p.u.)	f_3 (MW)	CPU time (s)
Multi-objective scenario-based stochastic optimization model (10 scenarios)	34698500	5.8168	2899.58	13489.2
Multi-objective scenario-based stochastic optimization model (20 scenarios)	34770400	5.8182	2907.91	29607.3
Multi-objective adaptive robust optimization model	34782500	5.8187	2909.12	2459.5
Proposed multi-objective robust optimization model	34841000	5.8203	2916.20	1725.4

For the multi-objective robust optimization model, the common methods to obtain the COS include weighted-sum method and C&CG algorithm (Method 1) as well as ε-constraint method and C&CG algorithm (Method 2). The comparative results with the above common methods and the proposed solution method are shown in Table XI.

TABLE XI
COMPARATIVE RESULTS OF VARIOUS METHODS FOR SOLVING PROPOSED MULTI-OBJECTIVE ROBUST OPTIMIZATION MODEL

Method	f_1 (¥)	f_2 (p.u.)	f_3 (MW)	d_+	d_-	CPU time (s)
Method 1	34970600	5.8637	2931.26	0.645	1.344	17528.6
Method 2	35011800	5.9329	2903.65	0.628	1.343	25430.2
Proposed solution method	34841000	5.8203	2916.20	0.602	1.381	1725.4

Among them, Method 2 takes the first objective as the main objective, while the other two objectives are considered as ε-constraints. The two ε values take 10 discrete points within the range of $[0,1]$, and lots of POSs are obtained by solving the proposed multi-objective robust optimization model corresponding to each combination of two ε values. Then, the POS with the minimum value of the two-layer optimization model in (50) is selected as the COS. In Method 1, the weight coefficients of each objective are evenly divided into 10 discrete points within $[0,1]$ to calculate POSs, and we select the COS with the minimum value of the two-layer optimization model in (50). Methods 1 and 2 need to obtain lots of discrete POSs. The proposed solution method can directly search for the COS in the entire feasible region, resulting in a shorter distance between the obtained COS and the utopia point, and a longer distance between the obtained COS and the nadir point, hence the obtained COS has a higher comprehensive optimization degree. In addition, compared with Method 1 and Method 2, even if both of them have used 8-core parallel computing to calculate the discrete POSs, the proposed solution method can still reduce the consumed CPU time by more than 90%, hence greatly increasing the computational efficiency.

B. Modified IEEE 39-bus Power System

The modified IEEE 39-bus power system divides the standard IEEE 39-bus system into two power grids with three B2B VSC systems. The three B2B VSC systems are connected at the end bus 39 of line 39-9, the end bus 3 of line 3-4, and the end bus 17 of line 17-16, respectively. In addition, buses 1 and 18 are connected with a wind farm and a photovoltaic station, respectively, as shown in Fig. 11. The predicted power output of both the wind farm and the photovoltaic station is 3 MW, with an uncertain fluctuation range of ±25%. $I_{f\max}$ is set to be 5 kA, and other parameters of the proposed multi-objective robust optimization model are consistent with Table I.

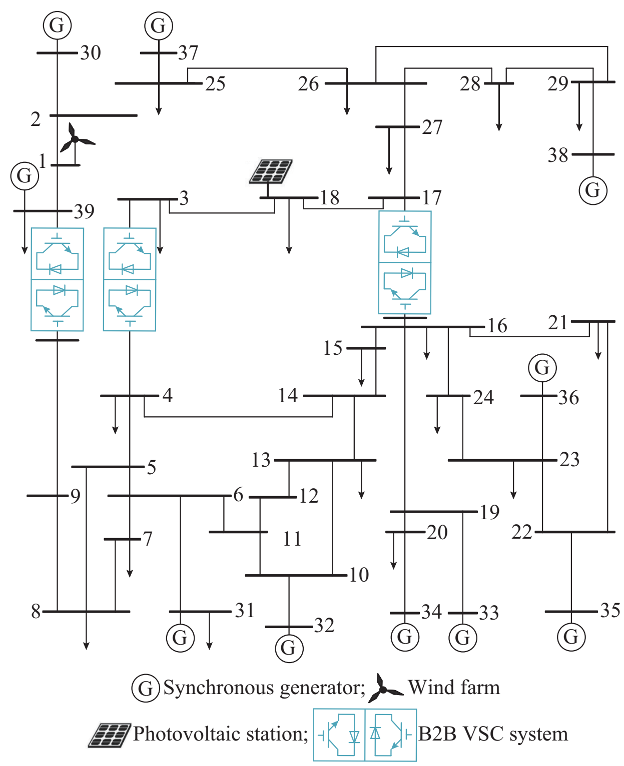

Fig. 11. Modified IEEE 39-bus power system.

The SCCs of three-phase short-circuit faults at each bus obtained by solving the optimization model without SCC constraints is shown in Fig. 12. It can be observed that the SCCs of buses 34, 36, and 38 exceed the upper limit.

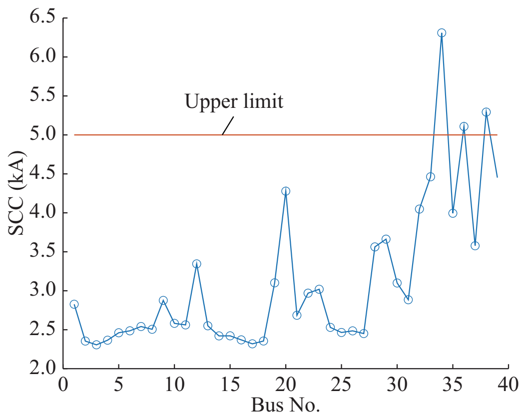

Fig. 12. SCCs of three-phase short-circuit faults at each bus without SCC constraints.

The three single-objective robust optimization models are solved, and the comparative results with and without B2B VSC systems are shown in Table XII. The obtained robust COS results and three single-objective robust optimization solutions are compared in Table XIII.

TABLE XII
RESULTS OF THREE SINGLE-OBJECTIVE ROBUST OPTIMIZATION MODELS WITH AND WITHOUT B2B VSC SYSTEM

Objective	Model	Optimal operation result	Objective value
min f_1	With B2B VSC		¥2106500
	Without B2B VSC	Generator 34 is shut-down	¥2211800
min f_2	With B2B VSC		0.0443 p.u.
	Without B2B VSC	Generator 36 is shut-down	0.0445 p.u.
min f_3	With B2B VSC		29.64 MW
	Without B2B VSC	Generator 34 is shut-down	32.62 MW

TABLE XIII
RESULTS OF OBTAINED ROBUST COS AND THREE SINGLE-OBJECTIVE ROBUST OPTIMIZATION SOLUTIONS

Objective	f_1 (¥)	f_2 (p.u.)	f_3 (MW)	d_+	d_-
min f_1	2106500	1.1166	57.45	1.029	1.393
min f_2	2283100	0.0443	502.33	1.414	1.000
min f_3	2156300	0.8071	29.64	0.766	1.264
Robust COS	2144700	0.2735	63.18	0.403	1.470

In addition, the SCCs of three-phase short-circuit faults at each bus corresponding to the obtained robust COS is shown in Fig. 13. It can be observed that the optimal operation mode can satisfy all SCC constraints with B2B VSC system. Compared with the model without B2B VSC system, the model with B2B VSC system has lower objective values and can reduce the number of shutdown generators, which is beneficial to the secure and economic operation of the system. Compared with the three single-objective robust optimization solutions, the obtained robust COS has the smallest distance from the utopia point, and the largest distance from the nadir point, which has the highest comprehensive optimization degree. The above conclusions are consistent with those of Section IV-A.

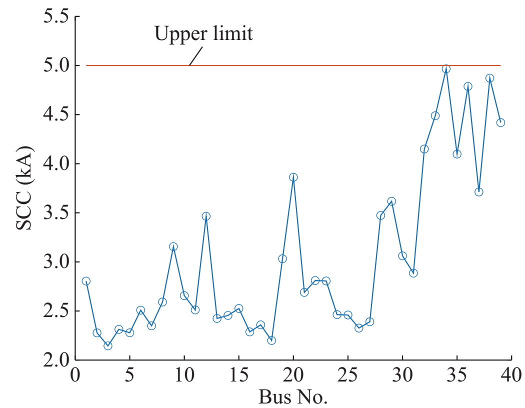

Fig. 13. SCCs of three-phase short-circuit faults at each bus corresponding to obtained robust COS.

VII. CONCLUSION

In order to limit SCC level in large-scale power grid, a multi-objective robust optimal secure operation model of power grid with B2B VSC systems considering the SCC limitation is proposed, and the following conclusions are obtained from the case studies of an actual 4407-bus provincial power grid and a modified IEEE 39-bus power system.

1) The multi-objective robust optimal secure operation model of power grid with B2B VSC systems can effectively limit the SCC level, reduce the numbers of shut-down generators and disconnection lines, and improve the secure operation and reliable power supply of power grids.

2) The MICP model with the inscribed N-sided approximation method to relax the nonlinear SCC limitation constraints has high computational efficiency in large-scale power grid, while ensuring high computational accuracy. The improved checking-adding-checking again-adding again method can reduce the CPU time by about 60%-70%, which is effective in addressing the problem that adding the SCC constraints of all buses directly is computationally intensive when applied to large-scale power grids.

3) The proposed solution method, combining the method to directly solve the COS and the C&CG algorithm, can reduce the consumed CPU time by more than 90% and obtain a better COS.

In the future power grid, as the penetration rate of RES increases, the effect of start-up and shut-down of renewable energy units, especially the grid-forming control base units, on SCC limitation may also be a future research direction.

REFERENCES

[1] H. Ye, S. Gao, G. Li *et al.*, "Efficient estimation and characteristic analysis of short-circuit currents for MMC-MTDC grids," *IEEE Transactions on Industrial Electronics*, vol. 68, no. 1, pp. 258-269, Jan. 2021.

[2] D. Yang, K. Zhao, and Y. Liu, "Coordinated optimization for controlling short circuit current and multi-infeed DC interaction," *Journal of Modern Power Systems and Clean Energy*, vol. 2, no. 4, pp. 374-384, Dec. 2014.

[3] H. Zhou, Y. Su, Y. Chen *et al.*, "The China southern power grid: solutions to operation risks and planning challenges," *IEEE Power and En-*

ergy Magazine, vol. 14, no. 4, pp. 72-78, Jul. 2016.

[4] H. Xie, R. Cao, Y. Song *et al*., "Research on the solution of voltage stability in Shenzhen during the asynchronous interconnection construction of Guangdong," in *Proceedings of 2023 IEEE 6th International Electrical and Energy Conference*, Hefei, China, May 2023, pp. 2855-2861.

[5] Z. Yang, H. Zhong, Q. Xia *et al*., "Optimal transmission switching with short-circuit current limitation constraints," *IEEE Transactions on Power Systems*, vol. 31, no. 2, pp. 1278-1288, Mar. 2016.

[6] J. Lin, Y. Hou, G. Zhu *et al*., "Co-optimization of unit commitment and transmission switching with short-circuit current constraints," *International Journal of Electrical Power & Energy Systems*, vol. 110, pp. 309-317, Sept. 2019.

[7] H. Hua, T. Liu, C. He *et al*., "Day-ahead scheduling of power system with short-circuit current constraints considering transmission switching and wind generation," *IEEE Access*, vol. 9, pp. 110735-110745, Aug. 2021.

[8] H. Hua, C. He, T. Liu *et al*., "On the solution to optimal topology adjustment in long-term power system operation with explicit short-circuit current limitation constraints," *IEEE Transactions on Power Systems*, vol. 39, no. 5, pp. 6764-6767, Sept. 2024.

[9] J. Wang, H. Zhong, Q. Xia *et al*., "Transmission network expansion planning with embedded constraints of short circuit currents and $N-1$ security," *Journal of Modern Power Systems and Clean Energy*, vol. 3, no. 3, pp. 312-320, Sept. 2015.

[10] H. Gharibpour, F. Aminifar, and M. H. Bashi, "Short-circuit-constrained transmission expansion planning with bus splitting flexibility," *IET Generation*, *Transmission & Distribution*, vol. 12, no. 1, pp. 217-226, Jan. 2018.

[11] H. Hua, T. Liu, X. Liu *et al*., "Optimal allocation and sizing of fault current limiters considering transmission switching with an explicit short circuit current formulation," *IEEE Transactions on Power Systems*, vol. 38, no. 2, pp. 1322-1335, Mar. 2023.

[12] M. Esmaili, M. Ghamsari-Yazdel, N. Amjady *et al*., "Short-circuit constrained power system expansion planning considering bundling and voltage levels of lines," *IEEE Transactions on Power Systems*, vol. 35, no. 1, pp. 584-593, Jan. 2020.

[13] M. Esmaili, M. Ghamsari-Yazdel, N. Amjady *et al*., "Transmission expansion planning including TCSCs and SFCLs: a MINLP approach," *IEEE Transactions on Power Systems*, vol. 35, no. 6, pp. 4396-4407, Nov. 2020.

[14] M. E. Parast, M. H. Nazari, and S. H. Hosseinian, "Resilience improvement of distribution networks using a two-stage stochastic multi-objective programming via microgrids optimal performance," *IEEE Access*, vol. 9, pp. 102930-102952, Jul. 2021.

[15] S. Zhang, S. Ge, H. Liu *et al*., "A multi-objective chance-constrained information-gap decision model for active management to accommodate multiple uncertainties in distribution networks," *Journal of Modern Power Systems and Clean Energy*, vol. 11, no. 1, pp. 17-34, Jan. 2023.

[16] G. Zhang, Y. Ge, X. Pan *et al*., "Hybrid robust-stochastic multi-objective optimization of combined cooling, heating, hydrogen and power-based microgrids," *Energy*, vol. 274, p. 127266, Jul. 2023.

[17] C. Zhang, Y. Xu, Z. Y. Dong *et al*., "Multi-objective adaptive robust voltage/var control for high-PV penetrated distribution networks," *IEEE Transactions on Smart Grid*, vol. 11, no. 6, pp. 5288-5300, Nov. 2020.

[18] Z. Yao, Z. Wang, and L. Ran, "Smart charging and discharging of electric vehicles based on multi-objective robust optimization in smart cities," *Applied Energy*, vol. 343, p. 121185, Aug. 2023.

[19] S. Zhang, S. Ge, H. Liu *et al*., "Distributionally robust hierarchical multi-objective voltage risk management for unbalanced distribution systems," *International Journal of Electrical Power & Energy Systems*, vol. 154, p. 109446, Dec. 2023.

[20] Y. Wang, M. Song, M. Jia *et al*., "Multi-objective distributionally robust optimization for hydrogen-involved total renewable energy CCHP planning under source-load uncertainties," *Applied Energy*, vol. 342, p. 121212, Jul. 2023.

[21] Z. Chu and F. Teng, "Short circuit current constrained UC in high IBG-penetrated power systems," *IEEE Transactions on Power Systems*, vol. 36, no. 4, pp. 3776-3785, Jul. 2021.

[22] W. Liang, S. Lin, J. Liu *et al*., "Multi-objective mixed-integer convex programming method for the siting and sizing of UPFCs in a large-scale AC/DC transmission system," *IEEE Transactions on Power Systems*, vol. 38, no. 6, pp. 5671-5686, Nov. 2023.

[23] X. Feng, S. Lin, W. Liu *et al*., "Distributionally robust optimal dispatch of offshore wind farm cluster connected by VSC-MTDC considering wind speed correlation," *CSEE Journal of Power and Energy Systems*, vol. 9, no. 3, pp. 1021-1035, May 2023.

[24] W. Feng, L. A. Tuan, L. B. Tjernberg *et al*., "A new approach for benefit evaluation of multiterminal VSC-HVDC using a proposed mixed AC/DC optimal power flow," *IEEE Transactions on Power Delivery*, vol. 29, no. 1, pp. 432-443, Feb. 2014.

[25] J. Liu, S. Lin, W. Liang *et al*., "Optimization for power distribution and maintenance schedules of paralleled transmission channels in AC/DC power system," *Journal of Modern Power Systems and Clean Energy*, vol. 12, no. 6, pp. 2030-2044, Nov. 2024.

[26] B. Zeng and L. Zhao, "Solving two-stage robust optimization problems using a column-and-constraint generation method," *Operations Research Letters*, vol. 41, no. 5, pp. 457-461, Sept. 2013.

[27] S. Lin, M. Liu, Q. Li *et al*., "Normalised normal constraint algorithm applied to multi-objective security-constrained optimal generation dispatch of large-scale power systems with wind farms and pumped-storage hydroelectric stations," *IET Generation*, *Transmission & Distribution*, vol. 11, no. 6, pp. 1539-1548, Apr. 2017.

Weikun Liang received the B. S. degree in electrical engineering from South China University of Technology, Guangzhou, China, in 2020. He is currently pursuing the Ph.D. degree with the School of Electric Power Engineering, South China University of Technology. His research interests include power system optimization, operation, and control.

Shunjiang Lin received the B. S. degree in electrical engineering from South China University of Technology, Guangzhou, China, in 2003, and the Ph. D. degree in electrical engineering from Hunan University, Changsha, China, in 2008. He is currently an Associate Professor with the School of Electric Power Engineering, South China University of Technology. His research interests include power system optimization, operation, and control.

Yuerong Yang received the B. S. degree in electrical engineering from South China University of Technology, Guangzhou, China, in 2019. He is currently pursuing the Ph.D. degree with the School of Electric Power Engineering, South China University of Technology. His research interests include power system optimization, operation, and control.

Ziqing Yang received the B.S. degree in electrical engineering from South China University of Technology, Guangzhou, China, in 2022. She is currently pursuing the M.S. degree with the School of Electric Power Engineering, South China University of Technology. Her research interests include power system optimization, operation, and control.

Mingbo Liu received the B.S. degree from Huazhong University of Science and Technology, Wuhan, China, in 1985, the M.S. degree from the Harbin Institute of Technology, Harbin, China, in 1988, and the Ph.D. degree from Tsinghua University, in 1992. He is currently a Professor with the South China University of Technology, Guangzhou, China. His research interests include power system optimization, operation, and control.